ARTICLES

SCIENCE CHINA Materials

mater.scichina.com link.springer.com

Published online 18 March 2020 | https://doi.org/10.1007/s40843-019-1259-6

Sci China Mater 2020, 63(6): 1076–1084

High-performance lateral MoS_2-MoO_3 heterojunction phototransistor enabled by *in-situ* chemical oxidation

Kaixi Bi[1], Qiang Wan[2], Zhiwen Shu[1], Gonglei Shao[3], Yuanyuan Jin[3], Mengjian Zhu[4], Jun Lin[2], Huawei Liu[2], Huaizhi Liu[1], Yiqin Chen[1], Song Liu[3*] and Huigao Duan[1*]

ABSTRACT **Construction of in-plane p-n junction with clear interface by using homogenous materials is an important issue in two-dimensional transistors, which have great potential in the applications of next-generation integrated circuit and optoelectronic devices. Hence, a controlled and facile method to achieve p-n interface is desired. Molybdenum sulfide (MoS_2) has shown promising potential as an atomic-layer n-type semiconductor in electronics and optoelectronics. Here, we developed a facile and reliable approach to *in-situ* transform n-type MoS_2 into p-type MoO_3 to form lateral p-n junction *via* a KI/I_2 solution-based chemical oxidization process. The lateral MoS_2/MoO_3 p-n junction exhibits a highly efficient photoresponse and ideal rectifying behavior, with a maximum external quantum efficiency of ~650%, ~3.6 mA W^{-1} at 0 V, and a light switching ratio of ~10^2. The importance of the built-in p-n junction with such a high performance is further confirmed by high-resolution photocurrent mapping. Due to the high photoresponse at low source-drain voltage (V_{DS}) and gate voltage (V_G), the formed MoS_2/MoO_3 junction p-n diode shows potential applications in low-power operating photodevices and logic circuits. Our findings highlight the prospects of the local transformation of carrier type for high-performance MoS_2-based electronics, optoelectronics and CMOS logic circuits.**

Keywords: molybdenum disulfide, lateral p-n junction, photocurrent, optoelectronics

INTRODUCTION

Two-dimensional (2D) semiconducting transition metal dichalcogenides (s-TMDCs) have attracted much attention due to their excellent physical properties, such as extreme thinness, high carrier mobility and direct band gap [1–6], which promote their widespread applications in post-silicon digital electronics and p-n diodes. The p-n diodes, including p-type and n-type s-TMDCs, are crucial to control the electrical properties of 2D electronic and optoelectronic devices [7–11]. Molybdenum sulfide (MoS_2), as the most studied s-TMDC, exhibits natural n-type due to the Fermi level pinning at the metal-MoS_2 interface, which limits its application in diodes. In order to get its p-n junction, developing controllable and reliable p-type doping techniques is desired. Several doping methods, including work function engineering, chemical doping, electrostatic doping and ionic gating, have been reported recently for TMDC p-n junctions and complementary devices [12–15]. Among them, the implant of p-type dopant into MoS_2 body *via* covalent bonding by chemical vapor deposition (CVD), for example, Nb-doped MoS_2, was reported to successfully transform n-type characteristics of MoS_2. However, the understanding about the growth mechanism and controllability is too limited to be applied in electronics. Chemical doping *via* small molecule physical adsorption on the surface is also a facile and common strategy, such as p-type doping realized on WSe_2 transistors by NO_2 adsorption [16]. Nevertheless, these approaches also have significant drawbacks, such as the air instability, low efficiency and controllability, and lattice damages. Transforming n-type TMDCs to p-type by chemical reaction provides a controllable and simple way to tune the carrier by *in situ* redox reaction. With $AuCl_3$ solution as the electron ac-

[1] College of Mechanical and Vehicle Engineering, State Key Laboratory of Advanced Design and Manufacturing for Vehicle Body, Hunan University, Changsha 410082, China
[2] School of Physics and Electronics, Hunan University, Changsha 410082, China
[3] Institute of Chemical Biology and Nanomedicine (ICBN), State Key Laboratory of Chemo/Biosensing and Chemometrics, College of Chemistry and Chemical Engineering, Hunan University, Changsha 410082, China
[4] College of Science, National University of Defense Technology, Changsha 410073, China
[*] Corresponding authors (emails: liusong@hnu.edu.cn (Liu S); duanhg@hnu.edu.cn (Duan H))

 © Science China Press and Springer-Verlag GmbH Germany, part of Springer Nature 2020

ceptor, Choi *et al.* [17] reported a p-type MoS_2 transistor based on the reduction reaction from $AuCl_4^-$ to Au.

Currently, p-n junctions are mainly established by CVD or vertical stacking *via* van der Waals force with mechanical transfer [17–23]. For vertical stacking, it is feasible to isolate, mix and match highly disparate atomic layers to create a wide range of van der Waals heterostructures with no lattice matching and processing compatibility. But it is difficult to control the spatial position precisely during assembly and get a sharp interface for the device integration. Synthesis of large-area TMDC heterostructures with an atomic-level thickness and well-defined structure has become attainable by CVD with spatial modulation of the chemical composition and electrical properties. Zhang *et al.* [21] have reported the growth of composition-tunable MoS_2-$MoSe_2$ lateral heterostructures by *in situ* vapor-phase reactant modulation and the fabricated lateral p-n diodes and photodiodes from the heterojunctions show high performances, which can be used to create complementary inverters with high voltage gain. However, in CVD growth, the 2D TMDCs need to meet the requirements of similar crystal structure and comparable lattice constant. It is still a big challenge to construct the lateral p-n junction with atomic sharp interface. Local doping by chemical reaction can be applied to construct p-n heterojunctions with high compatibility on homogenous materials. It can create atomically sharp interfaces with a controllable and simple process.

MoO_3 has been demonstrated as a candidate p-type doping material in organic and inorganic transistors [24–28]. Chuang *et al.* [14] have proven that p-type MoS_2 transistors could be formed by adding a substoichiometric molybdenum trioxide (MoO_x, $x < 3$) hole injection layer. Inspired by this, here, we employed the chemical reaction to *in situ* transform n-type MoS_2 partially to p-type MoO_3 under chemical oxidation by KI/I_2 solution and further modulated the conductivity to create a lateral homogenous p-n diode with an ideal rectifying behavior. Raman characterization and electrical measurements demonstrate the p-type doping. The p-n diode with an atomic interface shows the potential in the depletion region for separating and driving the electron-hole pairs for high photocurrent (3.6 mA W^{-1}) at zero bias. The device exhibits a high maximum external quantum efficiency (EQE), photoresponsibility, specific detectivity and inverting amplification gain. Our results promise a facile approach to chemical doping of MoS_2 transistors, and thus effectively tailoring their electrical properties for the realization of high-performance TMDC-based complementary electronic and optoelectronic devices.

METHODS

Synthesis of MoS_2 films

The MoS_2 films were synthesized on SiO_2/Si substrates in a hot-wall furnace (OTF-1200x-50) by CVD. High-purity MoO_3 (99%, Aldrich) and S powder (99.5%, Alfa) were placed in two separate Al_2O_3 crucibles, and the substrates were faced down and placed on the upper side of MoO_3 powder. The MoS_2 samples were prepared by annealing at 650°C for 15 min with a heating rate of 10°C min^{-1} in Ar atmosphere with 40 sccm flow rate.

Construction of p-n diode by KI/I_2 solution

KI/I_2 solution was prepared as the following procedure. Firstly, 4 g of KI (99%, Guangdong Chemicals) and 1 g of I_2 (99%, Guangdong Chemicals) were added into a glass container. Subsequently, 40 mL of denionized (DI) water was poured into the above solution till all the solids were dissolved under agitation. Polymethyl methacrylate (PMMA) (950 A6) was firstly spin-coated on the MoS_2 sample and baked on a hot plate at 180°C for 2 min. Subsequently, electrode patterns (5/50 nm Ti/Au) were defined by an electron beam lithography (EBL) system (Raith-150 TWO, Raith Company) and electron beam evaporation through a traditional lift-off process. After that, the PMMA resist was spin-coated on the device again with the same steps described above. Hydrogen silsesquioxane (HSQ) resist was spin-coated on the surface of MoS_2 device. And an overlay exposure of HSQ patterning was conducted by the EBL system at an accelerating voltage of 30 kV and a beam current of 310 pA. Square-like structures were realized at a typical area dose of 4000 μC cm^{-2}. The development of HSQ resist was achieved in a salty solution (1% NaOH + 4% NaCl in DI water) at 22°C for 1 min and then thoroughly rinsed by DI water for 1 min. Based on the protection of HSQ template, the channel material (MoS_2) was exposed partly to get a window for the oxidization process with KI/I_2 solution. Then some drops with KI/I_2 solution were put onto the surface of the device in air atmosphere for 1 min. Finally, the samples were rinsed by DI water for a few minutes to remove the residue, and then dried by a steady stream of nitrogen.

Electrical and optoelectrical measurements

Electrical measurements of the devices were performed by using a Keithley 4200 Semiconductor Parametric Analyzer and a Signotone Micromanipulator EPS150COAX

© Science China Press and Springer-Verlag GmbH Germany, part of Springer Nature 2020

probe station (Germany, Cascade Microtech). A light-emitting diode (LED) marked with white light was attached to the microscope of the probe station as the light source. The samples were kept at room temperature in ambient atmosphere during the measurements.

Photoresponsibility and temporal response times were measured under short-pulsed laser at a wavelength of 405 nm from a four-channel laser controller by using an Agilent A33220A waveform generator. Photocurrent mapping was performed by using a Pico Femto Integrated Source Measurement Unit and a Raman Witec alpha 300R system. The incident laser for generating the photocurrent was a diode-pumped solid-state laser (λ_{ex} = 532 nm). A focused laser with an optical lens of 50× magnification and a numerical aperture of 0.75 NA was used with the focused laser spot size of approximately 0.7 μm.

Characterization

The surface chemical structure of CVD MoS_2 was characterized by X-ray photoelectron spectroscopy (XPS, Thermo Fisher Scientific K-Alpha 1063). The crystal phase structure was examined by powder X-ray diffraction (XRD, Bruker Focus D8 diffractometer with Cu Kα radiation λ=0.15418 nm). Raman and photoluminescence (PL) spectra were obtained by Confocal Raman Microscopic systems (Alpha 300 R-WITec, Germany). Wavelength and spot size of the laser were 532 nm and 0.7 μm, respectively. The Si peak at 520 cm^{-1} was used for calibration in the experiments.

RESULTS AND DISCUSSION

MoO_3 is a widely used p-type doping candidate due to the high work function (the electron affinity for MoO_3 is 4.2 eV), while MoS_2 is a typical n-type semiconductor featured with low work function (the electron affinity for MoS_2 is 2.3 eV). Therefore, it is possible to convert n-type MoS_2 to p-type MoO_3 by partial oxidation reaction as shown in Fig. 1a. KI/I_2 in DI water can form highly oxidizing I_3^-, which can be used as the oxidation reagent. In order to prove this, MoS_2 field-effect transistors (FETs) were fabricated as standard fabrication methods and treated by KI/I_2 solution, as shown in Fig. S1 [29,30]. Briefly, MoS_2 film was connected by the source-drain contacts with Ti/Au (5/50 nm) by using standard electron beam lithography and e-beam evaporation. The electrical transport properties of the same MoS_2 transistor before and after KI/I_2 solution treatment were collected. As shown in Fig. 1b, monolayer MoS_2 exhibits n-type gate voltage (V_G) dependency on the source-drain current (I_{DS}) (black line). After treatment by KI/I_2, I_{DS} decreased with increasing V_G, showing a heavily p-doped behavior, and the mobility of charge carriers in MoS_2 before and after KI/I_2 treatment is 5.43 and 0.637 $cm^2\ V^{-1}\ S^{-1}$, respectively. The optical images of MoS_2 device before and after treatment with KI/I_2 are shown in insets of Fig. 1b. Besides, restricted by base-line noise and test limits in air atmosphere and equipment, the electrical data of MoS_2 sheets have a high off-state current, which leads to a low on/off ratio.

To further understand the conversion of MoS_2 transistor from n-type to p-type, Raman spectroscopy was applied to monitor the KI/I_2 treatment. As presented in Fig. 1c, the two intense peaks at 384 and 402 cm^{-1} are corresponding to E_{2g}^1 and A_{1g} modes of MoS_2, indicating MoS_2 still exists after KI/I_2 treatment [31,32]. Besides, some Raman peaks located at 161, 300, 384, 657 and 811 cm^{-1} appear and all the peaks correspond to α-MoO_3. The peaks positioned at 900–600 and 400–200 cm^{-1} regions are associated with Mo–O stretching and bending vibration modes, respectively. The absorption peaks at 811 cm^{-1} are the characteristics of α-MoO_3. PL spectrum after treatment exhibits clear blue shift and drastically enhanced intensity with time increasing, showing significant p-type doping effect, as shown in Fig. S2. The corresponding PL blue shift and intensity enhancement are associated with the switching of the dominant PL process from the recombination of negative trion to recombination of exciton under extraction of residual electrons in monolayer MoS_2. All the results confirm the existence of α-MoO_3 after KI/I_2 treatment and partial S in MoS_2 is oxidized by the highly oxidizing I_3^- under atmosphere in solution.

In order to further confirm the crystal structure of MoS_2 after KI/I_2 solution treatment, XRD analysis was conducted [33,34]. As shown in Fig. 1e, the XRD data were collected based on CVD-grown triangle MoS_2 film on silicon substrate. XRD pattern of MoS_2 (black line) shows hexagonal single crystal phase and crystalline without any impurities (JCPDS-37-1492). The characteristic peak of MoS_2 nanosheet is located at 14.5°, corresponding to (200) plane. The peaks at 18.5°, 26.2°, 33.0°, and 37.5° correspond to (111), (001), (101), and (200) planes of Si from the substrate. After KI/I_2 treatment, new XRD peaks at 44.9°, 52.2°, 58.9°, and 65.1° appear, which correspond to (200), (221), (171), and (062) planes of MoO_3. These results clearly demonstrate the chemical oxidation from MoS_2 to MoO_3 by KI/I_2.

XPS was also used to investigate the chemical states of Mo and S before and after oxidization (Fig. 1e, f). For

© Science China Press and Springer-Verlag GmbH Germany, part of Springer Nature 2020

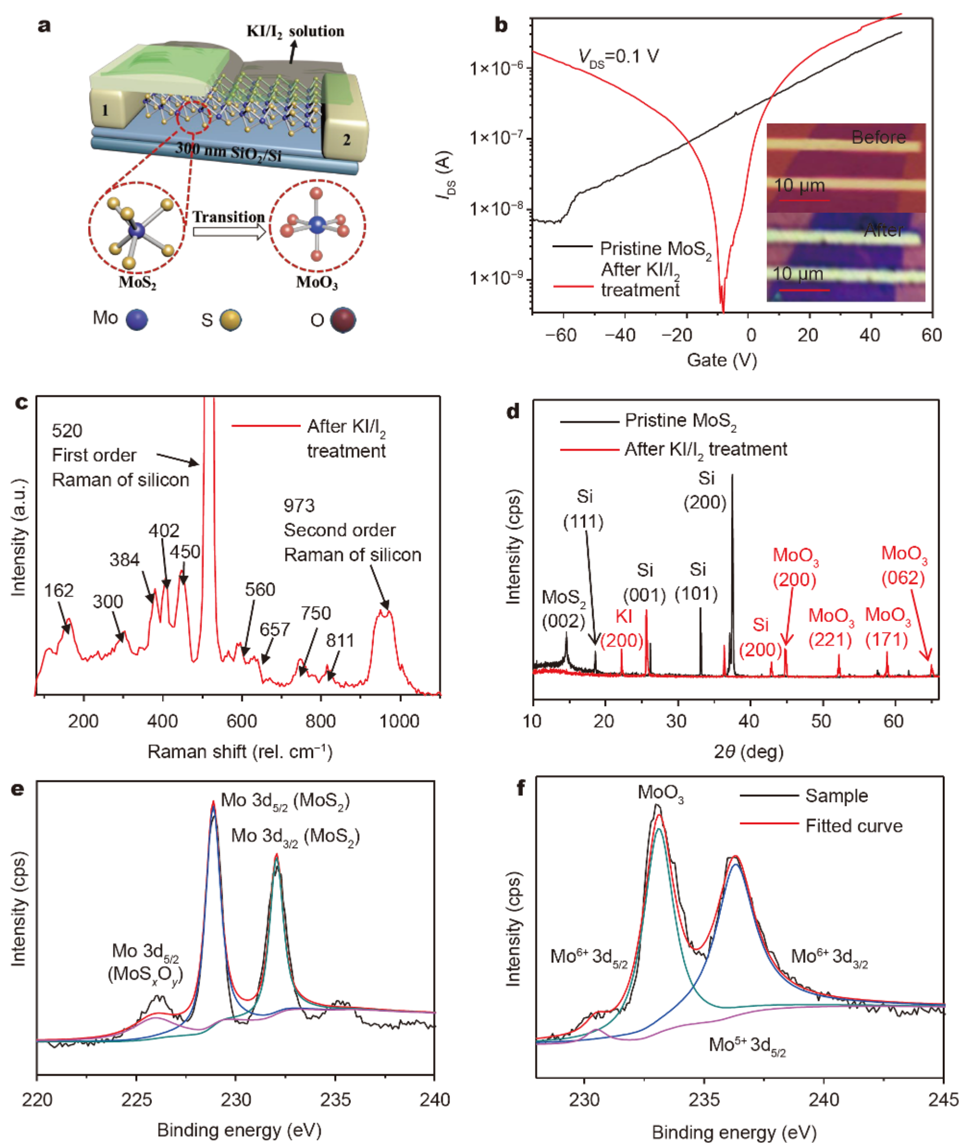

Figure 1 (a) Schematic illustration of MoS_2 thin film transistor oxidized by KI/I_2. (b) The transfer characteristic curves of MoS_2 device before and after treatment with KI/I_2. Insets: the optical images of MoS_2 device before and after treatment with KI/I_2. (c) Raman spectrum of CVD MoS_2 after KI/I_2 treatment. XRD pattern (d) and XPS spectra (e, f) of CVD-growth triangle MoS_2 film before and after treatment with KI/I_2.

CVD-grown MoS_2, the high-resolution XPS spectrum shows the binding energies of Mo $3d_{3/2}$ and Mo $3d_{5/2}$ are located at 232.8 and 229.6 eV, respectively, which are attributed to Mo^{4+} in MoS_2. Due to the inadequate reaction in CVD growth, the weak signal of binding energy located at 226.0 eV of Mo $3d_{5/2}$ indicates some products such as MoS_xO_y exist in the sample. After the sample was treated by KI/I_2 solution in the atmosphere, the absence of peaks at 232.8 and 229.6 eV indicates the oxidation of MoS_2. The binding energy peaks of Mo $3d_{5/2}$ and Mo $3d_{3/2}$ located at 233.1 and 236.2 eV clearly show MoO_3 crystal is produced. Considering all the results above, n-type MoS_2 was oxidized to p-type MoO_3 after KI/I_2 solution treatment.

Since n-type MoS_2 was partially oxidized into p-type MoO_3 by KI/I_2 solution, next we could locally treat the sample and construct the p-n junction in one piece of MoS_2 flake as shown in Fig. 2a. As a significant building block, p-n junction is one of the indispensable structures offered by the semiconductor technology in electronics. The basic working principle of p-n junction is shown in Fig. 2b, in which a built-in electric field is formed due to

 © Science China Press and Springer-Verlag GmbH Germany, part of Springer Nature 2020

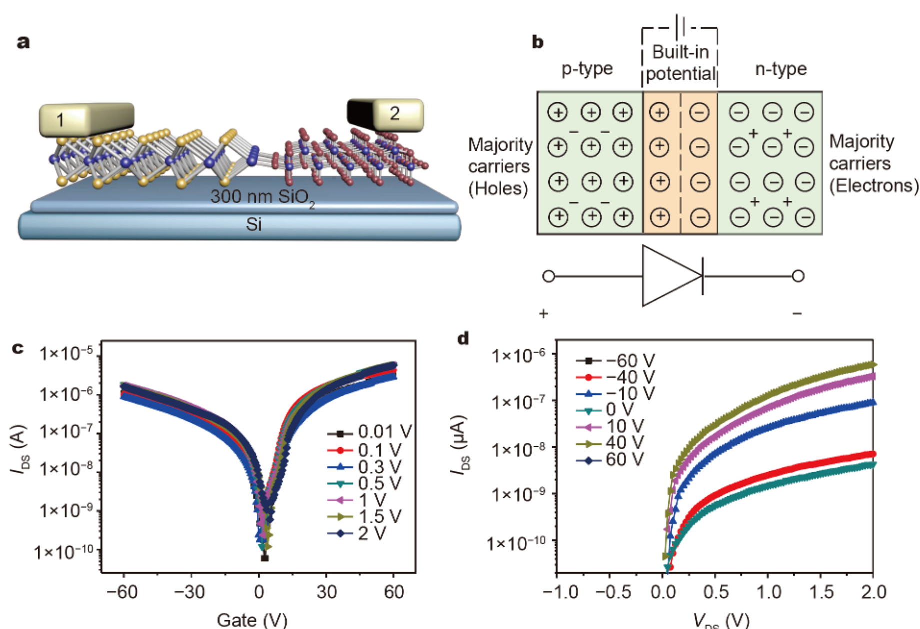

Figure 2 (a) Schematic illustration of a back-gated MoS_2 device partially oxidized by KI/I_2. (b) Basic working principle of p-n junction. (c) Transfer characteristic curves at different voltage bias of the partially oxidized MoS_2 device. (d) Output characteristics of the device after oxidization at different gate voltages.

the electron and hole diffusion, causing the electrons to flow exclusively in one direction and across it. Based on its properties, the structure can be used as semiconductor diode for rectification in the applications in LEDs, analog and digital circuits (ICs) [35–38].

We protected half channel of MoS_2 transistor by HSQ and exposed the other half channel treated by KI/I_2 to construct the p-n junction device. A series of transfer curves of the device are collected and shown in Fig. 2c. In the test range of V_G from −60 to 60 V, KI/I_2 partially treated MoS_2 FETs exhibit ambipolar transport property with both n-type and p-type characteristics. The rectifying property observed in these diodes can be attributed to MoO_3-induced (produced through the oxidizing reaction between KI/I_2 and MoS_2) p-type doping. The stronger p-doping is expected to result in a larger built-in potential barrier in the p-n junction, and thus bring about a higher rectification degree of the diode.

Fig. 2d further depicts the typical *I-V* curves of the p-n heterojunction measured in the dark, revealing an excellent rectification characteristic with a rectification ratio up to ~10^2 with V_{DS} varying from −1 to 2 V (log-scale I_{DS}-V_G curves shown in Fig. S3). From the rectification curve, a low turn-on voltage of 0.8 V can be deduced at the forward bias direction. The ideal rectification ratio and low turn-on voltage may associate with the acceptable contact resistance between the metal and semiconductor at low bias. In addition, the high-quality lattice match between the MoO_3 and MoS_2 interface leads to a low defect density, which is also helpful to the larger rectification factor.

The p-n junctions show attractive applications in optoelectronics. As shown in Fig. 3a, according to the band structure between n-type MoS_2 and p-type MoO_3, the built-in potential can be used for high-performance photodetector. MoO_3 traps electrons and MoS_2 traps holes in the boundary because of the work function difference between MoO_3 and MoS_2. Originating from the increase of electron concentration in MoO_3, Fermi level of MoS_2 moves closer to the conduction band edge, and significant charge transfer causes downward band bending. This phenomenon is very important for the application in logic circuits and high-performance optoelectronics based on p-n junction [38,39].

In Fig. S4, a series of different powers of 405 nm laser were employed on the MoS_2/MoO_3 heterostructure, in which more hole and electron carriers were induced between source and drain due to the irradiation of laser. The EQE can be calculated based on EQE = $(I_{ph}/P_{laser}) \times (hc/e\lambda)$, where P_{laser} is the absorbed laser power, I_{ph} is the photocurrent ($I_{ph}=I_{illumination}-I_{dark}$), h is the Planck constant, e is the electron charge, c is the velocity of light, and

 © Science China Press and Springer-Verlag GmbH Germany, part of Springer Nature 2020

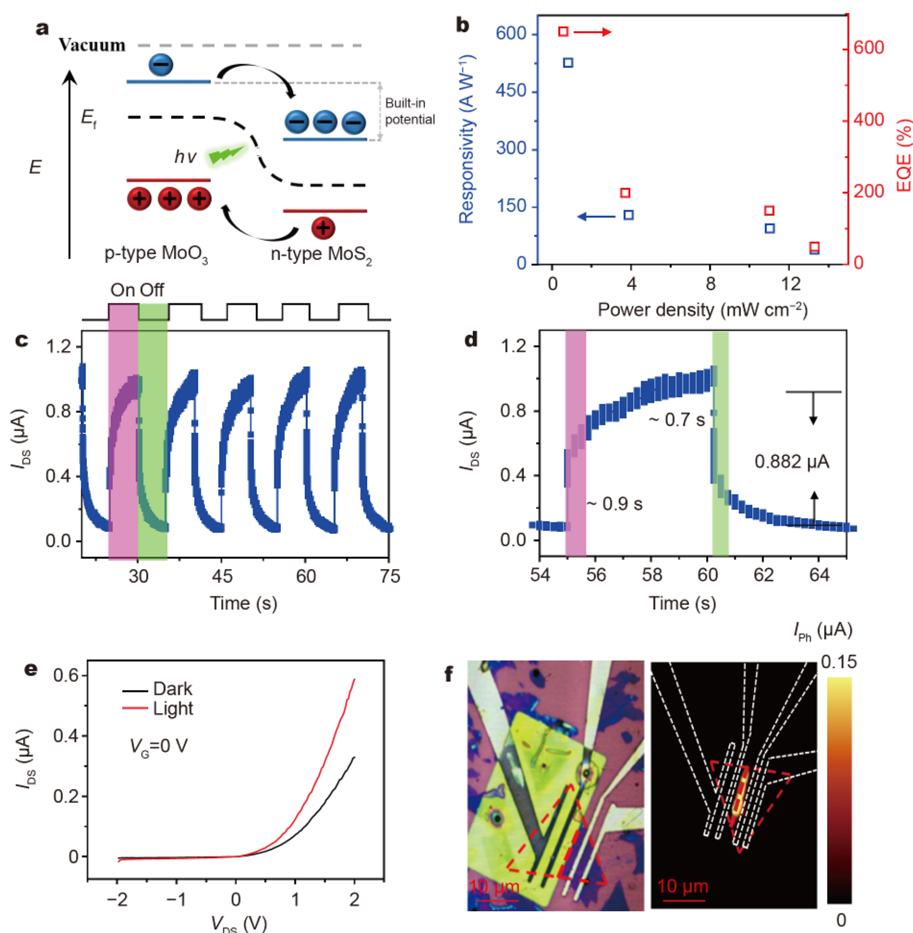

Figure 3 Photoresponse of MoS_2/MoO_3 p-n junction. (a) Band gap and band alignment at the MoS_2/MoO_3 interface. The electron affinity for MoS_2 and MoO_3 is 4.2 and 2.3 eV. (b) Calculated EQE and R with respect to the wavelength of light at V_{DS}= 0.1 V and V_G= ± 60 V. All the calculations were based on the data shown in Fig. S4. (c) Stability test of the photo-switching behavior of the MoS_2/MoO_3 heterojunction for pulsed light irradiation. (d) Enlarged photoswitching rising and falling edges for calculating the rise and fall times. (e) I_{DS}-V_{DS} characteristics of the device in dark (black) and under illumination of a white light (red) at zero back-gate bias. (f) Corresponding photocurrent image of the partially treated MoS_2 device under illumination of focused 532 nm laser at the boundary (red dashed line) between the MoS_2 and MoO_3. The photocurrent is extracted at zero drain voltage and zero gate voltage. The red triangle dashed line is the outline of MoS_2 flake. The white dashed lines are the outlines of electrodes. The left is the optical picture of the device.

λ is the laser wavelength. The calculated maximum EQE value of the device is 650% (V_{DS} = −1 V). To the best of our knowledge, this is a considerable result for photoresponsibility (R=I_{ph}/P_{laser}), and even it has a very sensitive R up to 527 A W^{-1} (all the data are summarized in Fig. 3b). It should be noted that the values of EQE and R decrease as the light power density resulting from the photocurrent of MoS_2/MoO_3 tends to get saturation.

The photoresponse of the MoS_2/MoO_3 heterojunction was further studied by modulating the incident light with a mechanical chopper as shown in Fig. 3c [40]. The data show the time dependence of short-circuit current I_{SC} at zero bias voltage (V_{DS} = 0 V) by periodically switching on and off the light. Significantly, the device works with excellent stability and reproducibility in manifold cycles. In Fig. 3d, the rise time (t_r) and fall time (t_f) correspond to times required for a photodetector to increase the photocurrent from 10% to 90% of its final value, and to decrease from 90% to 10% of its initial value, respectively. The MoS_2/MoO_3 heterojunction reveals a small rise time of ~0.9 s, as well as a fall time of ~0.7 s, which represent a considerable response speed for MoS_2-based photodetectors with different device structures and fabrication approaches. Compared with photo-switching of pristine CVD MoS_2 (Fig. S5), the fast photoresponse could be attributed to the high-quality p-n junction interface

 © Science China Press and Springer-Verlag GmbH Germany, part of Springer Nature 2020

formed between MoO_3 and MoS_2, in which photo-generated carriers could be quickly separated by the built-in electric field and then transfer to the electrodes. The linear I_{DS}-V_{DS} curves of the partially oxidized MoS_2 transistor in the dark (black) and under illumination of a white light (red) are displayed in Fig. 3e (the semi-log curves is provided in Fig. S6). The diode-like characteristic in black curve implies the successfully formed p-n junction in MoS_2 FET. In order to identify the origin of photocurrent and determine the local position of the p-n junction, high resolution photocurrent imaging under illumination of a focused 532 nm laser was carried out on the device and shown in Fig. 3f. The corresponding optical image is also provided in Fig. 3f. The laser power is ~50 μW with a ~700 nm spot illuminating at the interface between KI/I_2-treated (p-type MoO_3) and untreated channel (n-type MoS_2), which indicates that the lateral p-n junction indeed resulted from the partial oxidation reaction. The maximum photosensitivity of the device is ~3.6 mA W^{-1} at zero drain voltage and zero gate voltage. MoS_2/MoO_3 based p-n heterojunction shows the potential applications in optoelectronics.

Complementary inverters are also an important application for p-n junction. The schematic structure of an inverter device is shown in Fig. 4a. The MoS_2 flake is selectively chemically oxidized by KI/I_2 solution to form p-type MoO_3. Fig. 4b demonstrates the transfer curves of the pristine MoS_2 FETs and after KI/I_2 treatment. The pink line (pristine) presents a V_{min} at ~−55 V, indicating the electron-dominating transport in MoS_2 FETs. After chemical oxidation, the transfer curve (blue line) demonstrates a V_{min} of ~28 V, indicating a hole-dominating transport caused by p-type MoO_3. The complementary device was explored by integrating the two different kinds of FETs. A back-gate voltage was applied as the input (V_{IN}) and the supply voltage (V_{DD}) was applied to the p-type FET. The voltage transfer characteristics of the MoS_2 inverter at different V_{DD} are shown in Fig. 4c, in which clear signal inversion appears with high output voltage (V_{OUT}) and low V_{IN} and vice versa. The inset presents its corresponding electric circuits. The direct current voltage gain ($g=\partial V_{OUT}/\partial V_{IN}$) was calculated and shown in Fig. 4d, and it can reach to ~4.2 at V_{DD}= 7 V. Our methods provide a general strategy to fabricate high-performance nanoscale optoelectronic (photodetector) and electronic (complementary inverters) devices based on the MoS_2/MoO_3 p-n heterostructure.

CONCLUSIONS

In summary, n-type MoS_2 transistor to p-type MoO_3

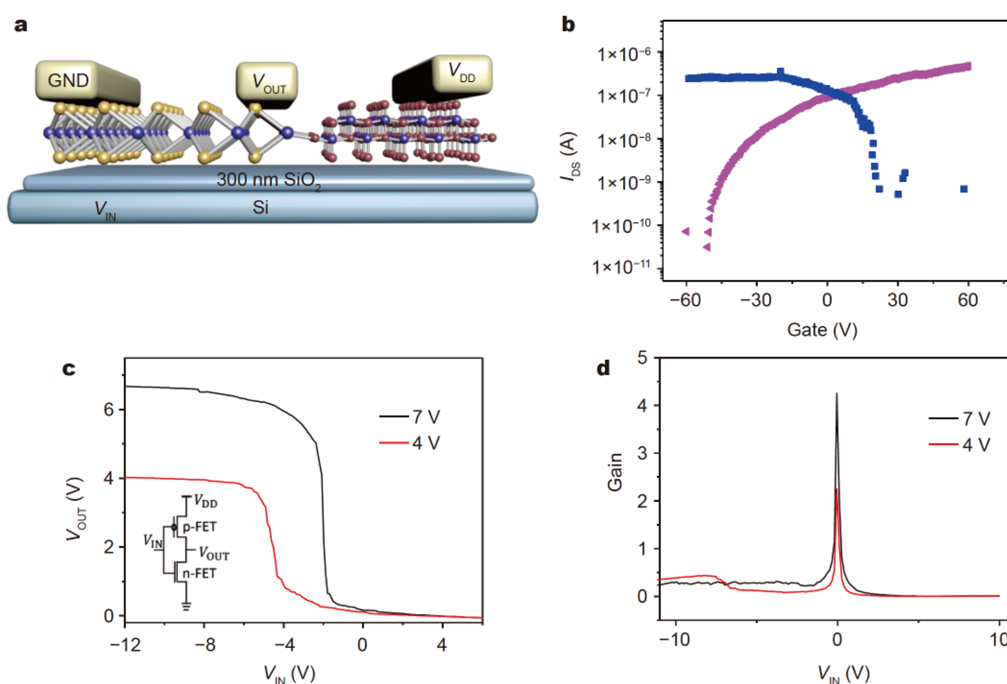

Figure 4 (a) The schematic structure of the inverter device. (b) Transfer characteristic of the pristine monolayer MoS_2 and chemical oxidized transistor. (c) Voltage-transfer characteristics of the MoS_2 CMOS inverter at different V_{DD}. Inset shows the circuit connections. (d) Direct-current voltage gain of the inverter at different V_{DD}.

 © Science China Press and Springer-Verlag GmbH Germany, part of Springer Nature 2020

transition had been successfully realized by chemical oxidation by treatment with KI/I_2 solution, and the stable MoS_2/MoO_3 p-n heterostructures with clear interface were constructed by partial oxidation in one flake *via* a controllable chemical treatment. The chemical oxidation mechanism was investigated to confirm the MoO_3 formation. The p-n junction was demonstrated to show a high-performance photoresponse and could be applied as the elemental unit for complementary device. Our results provide not only a powerful candidate approach for p-type doping 2D materials, but also a deeper understanding of the transformation from n-type to p-type. This method will pave a way for high-performance MoS_2-based electronics, optoelectronics and CMOS logic circuits.

Received 23 December 2019; accepted 21 January 2020; published online 18 March 2020

1 Yoon Y, Ganapathi K, Salahuddin S. How good can monolayer MoS_2 transistors be? Nano Lett, 2011, 11: 3768–3773
2 Zhou C, Wang X, Raju S, *et al.* Low voltage and high ON/OFF ratio field-effect transistors based on CVD MoS_2 and ultra high-k gate dielectric PZT. Nanoscale, 2015, 7: 8695–8700
3 Chang HY, Yang S, Lee J, *et al.* High-performance, highly bendable MoS_2 transistors with high-k dielectrics for flexible low-power systems. ACS Nano, 2013, 7: 5446–5452
4 Lu CC, Lin YC, Yeh CH, *et al.* High mobility flexible graphene field-effect transistors with self-healing gate dielectrics. ACS Nano, 2012, 6: 4469–4474
5 Liu Y, Guo J, Wu Y, *et al.* Pushing the performance limit of sub-100 nm molybdenum disulfide transistors. Nano Lett, 2016, 16: 6337–6342
6 Mustafeez W, Majumdar A, Vučković J, *et al.* A direct measurement of the electronic structure of Si nanocrystals and its effect on optoelectronic properties. J Appl Phys, 2014, 115: 103515
7 Liu Y, Ang KW. Monolithically integrated flexible black phosphorus complementary inverter circuits. ACS Nano, 2017, 11: 7416–7423
8 Britnell L, Gorbachev RV, Jalil R, *et al.* Field-effect tunneling transistor based on vertical graphene heterostructures. Science, 2012, 335: 947–950
9 Georgiou T, Jalil R, Belle BD, *et al.* Vertical field-effect transistor based on graphene–WS_2 heterostructures for flexible and transparent electronics. Nat Nanotech, 2012, 8: 100–103
10 Yu WJ, Liu Y, Zhou H, *et al.* Highly efficient gate-tunable photocurrent generation in vertical heterostructures of layered materials. Nat Nanotech, 2013, 8: 952–958
11 Britnell L, Ribeiro RM, Eckmann A, *et al.* Strong light-matter interactions in heterostructures of atomically thin films. Science, 2013, 340: 1311–1314
12 Laskar MR, Nath DN, Ma L, *et al.* p-Type doping of MoS_2 thin films using Nb. Appl Phys Lett, 2014, 104: 092104
13 Cuong NT, Otani M, Okada S. Gate-induced electron-state tuning of MoS_2: first-principles calculations. J Phys-Condens Matter, 2014, 26: 135001
14 Chuang S, Battaglia C, Azcatl A, *et al.* MoS_2 p-type transistors and diodes enabled by high work function MoO_x contacts. Nano Lett, 2014, 14: 1337–1342
15 Zhang YJ, Ye JT, Yomogida Y, *et al.* Formation of a stable p–n junction in a liquid-gated MoS_2 ambipolar transistor. Nano Lett, 2013, 13: 3023–3028
16 Zhao P, Kiriya D, Azcatl A, *et al.* Air stable p-doping of WSe_2 by covalent functionalization. ACS Nano, 2014, 8: 10808–10814
17 Choi MS, Qu D, Lee D, *et al.* Lateral MoS_2 p–n junction formed by chemical doping for use in high-performance optoelectronics. ACS Nano, 2014, 8: 9332–9340
18 Yu WJ, Li Z, Zhou H, *et al.* Vertically stacked multi-heterostructures of layered materials for logic transistors and complementary inverters. Nat Mater, 2013, 12: 246–252
19 Sup Choi M, Lee GH, Yu YJ, *et al.* Controlled charge trapping by molybdenum disulphide and graphene in ultrathin heterostructured memory devices. Nat Commun, 2013, 4: 1624–1631
20 Lim JY, Kim M, Jeong Y, *et al.* van der Waals junction field effect transistors with both n- and p-channel transition metal dichalcogenides. npj 2D Mater Appl, 2018, 2: 37
21 Zhang Z, Chen P, Duan X, *et al.* Robust epitaxial growth of two-dimensional heterostructures, multiheterostructures, and superlattices. Science, 2017, 357: 788–792
22 Duan X, Wang C, Shaw JC, *et al.* Lateral epitaxial growth of two-dimensional layered semiconductor heterojunctions. Nat Nanotech, 2014, 9: 1024–1030
23 Fan X, Zhao Y, Zheng W, *et al.* Controllable growth and formation mechanisms of dislocated WS_2 spirals. Nano Lett, 2018, 18: 3885–3892
24 Park GD, Choi SH, Kang YC. Electrochemical properties of ultrafine TiO_2-doped MoO_3 nanoplates prepared by one-pot flame spray pyrolysis. RSC Adv, 2014, 4: 17382–17386
25 Yin Z, Zhang X, Cai Y, *et al.* Preparation of MoS_2-MoO_3 hybrid nanomaterials for light-emitting diodes. Angew Chem Int Ed, 2014, 12560: 12565
26 Sharma RK, Reddy GB. Synthesis and characterization of α-MoO_3 microspheres packed with nanoflakes. J Phys D-Appl Phys, 2014, 47: 065305
27 Seguin L, Figlarz M, Cavagnat R, *et al.* Infrared and Raman spectra of MoO_3 molybdenum trioxides and $MoO_3{\cdot}xH_2O$ molybdenum trioxide hydrates. Spectrochim Acta Part A-Mol Biomol Spectr, 1995, 51: 1323–1344
28 Im H, Liu N, Bala A, *et al.* Large-area MoS_2-MoO_x heterojunction thin-film photodetectors with wide spectral range and enhanced photoresponse. APL Mater, 2019, 7: 061101
29 Gabette L, Segaud R, Fadloun S, Avale X, Besson P. Gold wet optimization on 200 mm substrates for MEMS application. ECS Trans, 2009, 25: 337–344
30 Sun S, Gao M, Lei G, *et al.* Visually monitoring the etching process of gold nanoparticles by KI/I_2 at single-nanoparticle level using scattered-light dark-field microscopic imaging. Nano Res, 2016, 9: 1125–1134
31 Vattikuti SVP, Nagajyothi PC, Reddy PAK, *et al.* Tiny MoO_3 nanocrystals self-assembled on folded molybdenum disulfide nanosheets *via* a hydrothermal method for supercapacitor. Mater Res Lett, 2018, 6: 432–441
32 Mestl G, Ruiz P, Delmon B, *et al.* Oxygen-exchange properties of MoO_3: an *in situ* Raman spectroscopy study. J Phys Chem, 1994, 98: 11269–11275
33 Li CQ, Shen X, Ding RC, *et al.* Controllable synthesis of one-dimensional MoO_3/MoS_2 hybrid composites with their enhanced

 © Science China Press and Springer-Verlag GmbH Germany, part of Springer Nature 2020

efficient electromagnetic wave absorption properties. ChemPlusChem, 2019, 84: 226–232

34 Pareek A, Kim HG, Paik P, *et al.* Ultrathin MoS_2–MoO_3 nanosheets functionalized CdS photoanodes for effective charge transfer in photoelectrochemical (PEC) cells. J Mater Chem A, 2017, 5: 1541–1547

35 Luo W, Zhu M, Peng G, *et al.* Carrier modulation of ambipolar few-layer $MoTe_2$ transistors by MgO surface charge transfer doping. Adv Funct Mater, 2018, 28: 1704539

36 Yoo G, Hong S, Heo J, *et al.* Enhanced photoresponsivity of multilayer MoS_2 transistors using high work function MoO_x overlayer. Appl Phys Lett, 2017, 110: 053112

37 Baugher BWH, Churchill HOH, Yang Y, *et al.* Optoelectronic devices based on electrically tunable p–n diodes in a monolayer dichalcogenide. Nat Nanotech, 2014, 9: 262–267

38 Patra KK, Ghosalya MK, Bajpai H, *et al.* Oxidative disproportionation of MoS_2/GO to MoS_2/MoO_{3-x}/RGO: integrated and plasmonic 2D-multifunctional nanocomposites for solar hydrogen generation from near-infrared and visible regions. J Phys Chem C, 2019, 123: 21685–21693

39 Yu SH, Lee Y, Jang SK, *et al.* Dye-sensitized MoS_2 photodetector with enhanced spectral photoresponse. ACS Nano, 2014, 8: 8285–8291

40 Zhang W, Huang JK, Chen CH, *et al.* High-gain phototransistors based on a CVD MoS_2 monolayer. Adv Mater, 2013, 25: 3456–3461

Acknowledgements We gratefully acknowledge the financial support from the National Natural Science Foundation of China (51722503, 51621004, 21705036 and 21975067), and the Natural Science Foundation of Hunan Province, China (2018JJ3035). The research has also received funding from the Fundamental Research Funds for the Central Universities from Hunan University.

Author contributions Duan H and Liu S conceived the ideas and designed the experiments; Bi K, Liu HW and Lin J engineered the samples; Wan Q, Shu Z and Shao G performed the XRD, XPS and Raman experiments. Bi K, Zhu M, Jin Y and Lin J fabricated and characterized the MoS_2 device with assistance from Liu HW, Chen Y and Liu HZ. Bi K wrote the manuscript with input from all co-authors. All authors discussed the results and commented on the manuscript.

Conflict of interest The authors declare no competing financial interest.

Supplementary information The schematic of device fabrication process, PL spectral change with time, photoresponses with different irradiation powers and the characterization of the control photoswitching of CVD MoS_2 are available in the online version of the paper.

Kaixi Bi received his PhD majored in physics from Hunan University in 2019. He is now a full-time lecturer at the School of Instrument and Electronics, North University of China. His current research interests include nanomanufacturing, low-dimensional material field effect transistors, smart micro/nanosystems and their relevant applications.

Song Liu received his PhD in 2011 from Peking University. He was a postdoctoral fellow working in Prof. Liming Dai's group (2011–2013) in Case Western Reserve University. After three years' research in National University of Singapore (2013–2016), he is now a full professor at the Institute of Chemical Biology and Nanomedicine, Hunan University. His research interests focus on the controlled synthesis of low-dimensional materials, the application research of functional devices and nanobiological research.

Huigao Duan received his BSc and PhD in physics from Lanzhou University (China) in 2004 and 2010, respectively. He joined Hunan University as a full professor in 2012 and then set up a micro/nanofabrication laboratory there. His current research interests include sub-10-nm patterning, high-resolution color printing, nanomanufacturing, smart micro/nanosystems and their relevant applications.

原位化学氧化构建高性能MoS_2-MoO_3面内同质异质结光敏晶体管

毕开西[1], 万强[2], 舒志文[1], 邵功磊[3], 靳媛媛[3], 朱梦剑[4], 林均[2], 刘华伟[2], 刘怀志[1], 陈艺勤[1], 刘松[3*], 段辉高[1*]

摘要 由组成相同的材料构建具有清晰边界的平面内p-n异质结是二维晶体管研究面临的主要挑战之一, 在下一代集成电路和光电器件领域具有重要的潜在应用. 因此有必要开发一种可实现p-n界面的简便、可控的操作方法. 硫化钼(MoS_2)作为一种具有原子层厚度的n型半导体材料已经在电子学和光电子学领域展现出巨大的应用前景. 在本研究中, 我们通过KI/I_2溶液化学氧化诱导方法实现了从n型MoS_2到p型MoO_3的原位转化, 进而形成了横向面内p-n异质结. MoS_2/MoO_3 p-n异质结显示出高效的光响应和整流特征, 0 V、~3.6 mA W^{-1}条件下最大外部量子产率达到~650%, 同时光开关比达到~10^2. 构筑的p-n异质结的高性能也被光电流面扫描所证实. 由于器件在低源漏电压(V_{DS})和栅压(V_G)条件下具有高的光响应性能, MoS_2/MoO_3 p-n二极管在光电器件及集成电路中的应用具有低功耗的特点. 本研究为局部进行载流子种类转变提供了可能的途径, 并将MoS_2进一步应用于电子学、光电子学及CMOS逻辑电路领域.

 © Science China Press and Springer-Verlag GmbH Germany, part of Springer Nature 2020